

Discharge impedance of solenoidal inductively coupled plasma discharge

K.-I. You and N. S. Yoon

Korea Basic Science Institute, Taejeon 305-333, Korea

(Received 11 December 1998)

The discharge impedance is calculated for a solenoidal inductively coupled plasma (ICP) discharge, which is one of the important sources for plasma processing. To calculate this impedance, the electromagnetic field quantities are obtained by solving the two-dimensional Maxwell equations in a realistic geometry. Also considered in the calculation is the anomalous skin effect which is regarded as a collisionless heating mechanism of ICP discharge. The results show that the discharge impedance is a function of various discharge parameters, such as plasma density, electron temperature, antenna position, collision frequency, excitation frequency, and chamber geometry. [S1063-651X(99)03706-X]

PACS number(s): 52.80.Pi, 52.50.-b, 52.75.-d

I. INTRODUCTION

The inductively coupled plasma (ICP) source has been the subject of many experimental and theoretical investigations [1–14]. Since a high-density plasma with good uniformity is easily obtained under low pressure without an external magnetic field, the ICP becomes a strong candidate for a next-generation source for plasma processing. Two types of ICP reactors are available, which are classified according to the shape and position of the coil. One type of the reactors has a solenoidal coil wound around the cylindrical chamber (solenoidal type) [1–9] and the other type has a planar coil at the top of the chamber (planar type, also called TCP) [10–14].

For the electron heating mechanism of the ICP discharge, collisionless heating is widely accepted as the primary mechanism, since it is sustained with low-pressure neutral gas. The collisionless electron heating mechanism is the anomalous skin effect originated from thermal motion of plasma particles [5,15]. The anomalous skin effect is a transverse analogue of the Landau damping from the standpoint of wave-particle interaction in plasma, since the electrons gain energy through a resonant coupling with the transverse electromagnetic waves.

Although the anomalous skin effect has been a traditional subject in plasma physics, many issues remain to be understood more fully, especially in relation to the collisionless heating mechanism of the ICP discharge. The recent progress is well reviewed in Refs. [9,16]. One of the important issues of the collisionless heating mechanism is the calculation of surface and plasma impedances, since they are the representative quantities of the heating mechanism. In the case of the TCP discharge, Yoon *et al.* [17] developed a one-dimensional model including the anomalous skin effect and the modulation effect of the wave electric field by conducting boundaries at the other side of the plasma. This model was extended to a two-dimensional model [18]. The surface impedance can be calculated from the one-dimensional model, and the plasma impedance from the two-dimensional model with the field definition of impedance [19]. For the solenoidal ICP discharge, the surface impedance was calculated by Sayasov [20] with a one-dimensional model, but the plasma impedance has not yet been fully calculated. There is no such calculation obtained for the discharge impedance.

One of two main difficulties in two-dimensional modeling is that the radial normal mode of the electron kinetic equation is not amenable to cooperation with the eigenmode of the wave equation. The other is the determination of excitation coefficients of the normal mode by the external coil current. In the work of Yoon, Hwang, and Choi [18], the first problem was overcome by assuming that the radius of plasma is much larger than the skin depth, as is often the case in the practical ICP discharge condition. For the second problem, an effective surface current representing the transverse magnetic field was introduced into the interface between plasma and vacuum as a tentative boundary condition. This surface current can be presented as a function of the antenna coil current by manipulating the Maxwell equations, and thus the excitation coefficients can be determined. The use of the effective surface current is justified by the uniqueness theorem of the solution. From the viewpoint of an electrical circuit model, an impedance matching condition is determined with the discharge impedance which is the impedance of the whole chamber. This discharge impedance can be calculated from the electromagnetic field quantities in the antenna region. The electromagnetic field in the plasma region is calculated easily with the method of Ref. [18]; the field in the antenna region, however, cannot be obtained.

In this work, we develop a two-dimensional heating theory of the solenoidal ICP discharge by representing the anomalous skin effect in terms of the conductivity of homogeneous hot plasma; for the calculation of the conductivity, electrons are assumed to reflect perfectly on the plasma boundary. The normal mode in the plasma region is represented with an effective surface current, and this surface current is determined by the antenna current not only with the method of Yoon *et al.* (hereafter called the mode excitation method), but also with the image current method. In the image current method, the wave equation is solved also in the antenna region by replacing the plasma current with an appropriate current sheet (which we call image current sheet) at a certain radial position in the plasma region. The image current and the electromagnetic field in both regions are determined, without loss of generality, by assuming that the electric and magnetic fields should be continuous at the plasma-vacuum boundary. Once the electromagnetic field is determined, the plasma impedance can be calculated from

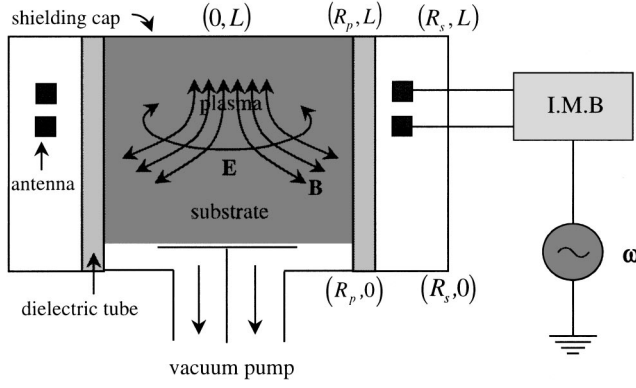


FIG. 1. Schematic diagram of a solenoidal ICP discharge device.

the field quantities [19] on the plasma-vacuum interface and the discharge impedance from those on the surface of the antenna. The resulting plasma and discharge impedances are functions of various parameters such as plasma density, electron temperature, radius of chamber, length of plasma, radius of plasma, electron collision frequency, excitation frequency, and the position and size of the antenna coil.

In Sec. II, the wave equation and boundary conditions are described and the solution is presented. The numerical results and discussion are presented in Sec. III, and the summary is given in Sec. IV.

II. THEORY

A. Wave equation and boundary conditions

Figure 1 shows a schematic diagram of a usual solenoidal ICP source, whose electromagnetic field and impedance are calculated. The dielectric tube filled with plasma has a radius of R_p and the antenna coil with radius R_c is wound around this dielectric tube. We define the plasma and antenna regions by the inner range $0 \leq r \leq R_p$ and the outer range $R_p \leq r \leq R_s$, respectively, where R_s is the chamber radius. Since the alternating current in the antenna coil generates time-varying magnetic flux in the plasma region, the azimuthal electric field is induced in the plasma. Electrons gain energy from this electric field through the resonant coupling and ionize the neutral gas.

In general, the electric field can be resolved into irrotational (longitudinal or capacitive) and solenoidal (transverse or inductive) parts. Two important roles of the capacitive field are to make a difference of the conduction current on the antenna from the input current as much as the displacement current in the perpendicular direction to the antenna surface, and to heat the plasma electrons (capacitive discharge). For the practical ICP discharge condition, however, the dominant electron heating source is the inductive part of the electric field rather than the capacitive part, and the capacitive field is usually Faraday shielded. Therefore, only the inductive field is considered in this work.

Assuming that all physical quantities have θ symmetry and the electric field \vec{E} has only a θ component ($\vec{E} = E \hat{\theta}$), the wave equation for the azimuthal electric field E in (r, z) coordinate system is written as

$$\left(\frac{\partial^2}{\partial r^2} + \frac{1}{r} \frac{\partial}{\partial r} - \frac{1}{r^2} + \frac{\partial^2}{\partial z^2} + \kappa^2 \right) E(r, z) = -i\kappa \frac{4\pi}{c} J(r, z), \quad (1)$$

where $\kappa = \omega/c$, ω is the excitation wave frequency, c the speed of light, and J the sum of all current densities appearing in the chamber. Here, the electric field and the current are assumed to depend on time in the form of $e^{-i\omega t}$. The components of the magnetic field can be calculated from E by using Faraday's law

$$B_r(r, z) = \frac{i}{\kappa} \frac{\partial}{\partial z} E(r, z), \quad (2)$$

$$B_z(r, z) = -\frac{i}{\kappa} \frac{\partial}{\partial r} [rE(r, z)], \quad (3)$$

and the absorption power density P_{abs} defined as the power absorbed by the plasma in unit volume is

$$P_{\text{abs}} = \frac{1}{2} \text{Re}(J_p^* E), \quad (4)$$

where J_p is the plasma current density.

The whole chamber is assumed to be surrounded with a perfect conductor; thus, $E=0$ at the chamber surface. Since it is not easy to solve Eq. (1) for the whole chamber, the wave equation is solved separately in each region and the solutions are matched at boundary without loss of generality. The wave equation in the plasma region is solved with a temporal boundary condition at the plasma-vacuum boundary:

$$B_z = B_p \quad \text{at } r = R_p. \quad (5)$$

To determine the value of B_p , we use two methods of mode excitation and image current.

In the mode excitation method, the electric and magnetic fields satisfying source-free wave equations in the antenna region are used in a vector relation derived from the Maxwell equations. Integrating this identity in the antenna region, B_p can be obtained as a function of the antenna current. In the image current method, the wave equation in the antenna region is also solved easily by replacing the plasma current with an image current sheet at a certain position within the plasma region. This image current and B_p are determined from the magnetic and the electric field continuity conditions at the plasma-vacuum boundary. The electromagnetic field in the antenna region can be obtained with the image current method, although the calculation in this method is more complex and time consuming than that based on the mode excitation method. The procedures of the mode excitation and image current methods should be guaranteed by the uniqueness theorem. The proof of uniqueness is offered by Yoon, Hwang, and Choi [18] for the case of the TCP discharge. Since the solenoidal ICP situation is not much different from the TCP case in proving the uniqueness theorem, the validity of the uniqueness theorem for the ICP is assumed without any proof. Owing to this uniqueness theorem, the results from the mode excitation and the image current methods can be cross-checked to examine if they are equal.

B. Normal mode in the plasma region

In the plasma region, the wave equation is written as

$$\left(\frac{\partial^2}{\partial r^2} + \frac{1}{r} \frac{\partial}{\partial r} - \frac{1}{r^2} + \frac{\partial^2}{\partial z^2} + \kappa^2\right)E = -i\kappa \frac{4\pi}{c} J_p, \quad (6)$$

with boundary conditions

$$E=0 \quad \text{at } r=0, \quad (7)$$

$$B_z = B_p \quad \text{at } r=R_p. \quad (8)$$

The homogeneous solution of Eq. (6) with the boundary condition given by Eq. (8) can be transformed into a particular solution with the effective surface current density K_s at R_p , and the equivalent wave equation becomes

$$\begin{aligned} &\left(\frac{\partial^2}{\partial r^2} + \frac{1}{r} \frac{\partial}{\partial r} - \frac{1}{r^2} + \frac{\partial^2}{\partial z^2} + \kappa^2\right)E \\ &= -i\kappa \frac{4\pi}{c} [J_p + K_s \delta(r-R_p)], \end{aligned} \quad (9)$$

where $\delta(r)$ is the Dirac delta function and $K_s = cB_p/2\pi$.

This equation can be solved by the mode analysis method using the Fourier-Dini series [21], and the results become

$$E = \sum_{m,n} e_{mn} J_1\left(\lambda_{0m} \frac{r}{R_p}\right) \sin(q_n z), \quad (10)$$

$$J_p = \sum_{m,n} e_{mn} \sqrt{2\pi} \sigma_{p,m} J_1\left(\lambda_{0m} \frac{r}{R_p}\right) \sin(q_n z), \quad (11)$$

where

$$e_{mn} = \frac{2i\kappa b_{p,n}}{R_p J_1(\lambda_{0m}) D_{mn}}, \quad (12)$$

$$D_{mn} = (\lambda_{0m}/R_p)^2 + q_n^2 - \kappa^2 - \frac{4\pi}{c} i\kappa \sqrt{2\pi} \sigma_{p,m}, \quad (13)$$

and J_1 is the first-order Bessel function and λ_{0m} are roots of the zeroth Bessel function J_0 satisfying $J_0(\lambda_{0m})=0$. Here, $q_n = n\pi/L$ with plasma length L , $\sigma_{p,m}$ is the m th coefficient of plasma conductivity σ_p in the Dini series and is given from the solution of the Boltzmann equation, and $b_{p,n}$ is the n th coefficient of B_p in the Fourier series defined by

$$b_{p,n} = \frac{2}{L} \int_0^L B_p \sin(q_n z) dz. \quad (14)$$

The remaining unknown $b_{p,n}$ will be obtained from the electric field continuity condition at the plasma-vacuum boundary.

The plasma conductivity is deduced from the Boltzmann equation for the electron velocity distribution function f , and the equation for the dominant order is

$$\frac{\partial f_1}{\partial t} + v_r \frac{\partial f_1}{\partial r} - \frac{e}{m} E \frac{\partial f_0}{\partial v_\theta} = \left(\frac{\partial}{\partial t}\right)_{\text{col}} f_1, \quad (15)$$

where f_0 and f_1 are the uniform equilibrium and perturbed distribution functions, respectively, and $(\partial/\partial t)_{\text{col}}$ is a collision operator. v_r , v_θ , e , and m are velocity components in radial and azimuthal directions, electron charge, and electron mass, respectively. Here, the axial derivative of the perturbed electron velocity distribution ($\partial f_1/\partial z$) is neglected on the assumption of $L \gg \delta$, where δ is the skin depth in the radial direction. Using the Maxwellian distribution function for f_0 and Krook's model collision operator, we have

$$-i(\omega + i\nu)f_1 + v_r \frac{\partial f_1}{\partial r} + \frac{e}{T_e} E v_\theta f_0 = 0, \quad (16)$$

where ν and T_e are the frequency of electron collision with neutral gas particles and the electron temperature, respectively. Following the procedure given in Ref. [20], Eq. (16) can be solved assuming that $R_p \gg \delta$ and electrons reflect perfectly from the plasma boundary. After some algebraic manipulation for f_1 , the plasma conductivity can be expressed by the Dini series and its component becomes

$$\sigma_{p,m} = -\frac{ie^2 n_p R_p}{2\sqrt{2\pi} T_e \lambda_{0m}} Z_p \left(\frac{\omega + i\nu}{\lambda_{0m} v_{\text{th}}/R_p}\right), \quad (17)$$

where Z_p , n_p , and v_{th} are the plasma dispersion function [22], plasma density, and electron thermal velocity, respectively.

C. Mode excitation method

In this subsection, we determine the magnetic field component at the plasma-vacuum boundary ($b_{p,n}$) [Eq. (14)], using the mode excitation method. By adopting this method, we connect the normal mode in the plasma region to the antenna current without solving the wave equation in the antenna region.

From the Maxwell equations, we derive a vector relation

$$\vec{\nabla} \cdot (\vec{E} \times \vec{B}_{\text{no}} - \vec{E}_{\text{no}} \times \vec{B}) = (4\pi/c) \vec{J}_c \cdot \vec{E}_{\text{no}}, \quad (18)$$

where J_c is the source current density, and the subscript no means the electromagnetic field satisfies the source-free wave equation

$$\left(\frac{\partial^2}{\partial r^2} + \frac{1}{r} \frac{\partial}{\partial r} - \frac{1}{r^2} + \frac{\partial^2}{\partial z^2} + \kappa^2\right)E_{\text{no}} = 0. \quad (19)$$

Here, $\vec{E}_{\text{no}} = E_{\text{no}} \hat{\theta}$, and the boundary condition for Eq. (19) is

$$E_{\text{no}} = 0 \quad \text{at } r=R_s. \quad (20)$$

The solution of Eq. (19) can be written as

$$E_{\text{no}} = \sum_n C_n g_n(r) \sin(q_n z), \quad (21)$$

with

$$g_n(r) = K_1(\beta_n R_s) I_1(\beta_n r) - I_1(\beta_n R_s) K_1(\beta_n r), \quad (22)$$

in which I_1 and K_1 are the first-order modified Bessel functions, and $\beta_n^2 \equiv q_n^2 - \kappa^2$. From the Maxwell equations, magnetic field \vec{B}_{no} becomes

$$\vec{B}_{\text{no}} = \frac{1}{i\kappa} \sum_n C_n [-q_n \cos(q_n z) g_n(r) \hat{r} + \beta_n \sin(q_n z) h_n(r) \hat{z}], \quad (23)$$

with

$$h_n(r) = K_1(\beta_n R_s) I_0(\beta_n r) + I_1(\beta_n R_s) K_0(\beta_n r), \quad (24)$$

I_0 and K_0 being the zeroth-order modified Bessel functions. With Eq. (18) volume integrated over the antenna region, an integral equation is obtained

$$\int_{r=R_p} (E_{\text{no}} B_z - B_{\text{no},z} E) R_p dz = \frac{4\pi}{c} \int_0^L \int_{R_p}^{R_s} J_c E_{\text{no}} r dr dz, \quad (25)$$

with assumption of $E=0$ at the chamber surface. Expanding B_z at R_p in the Fourier series

$$B_z(R_p) = \sum_n b_{p,n} \sin(q_n z), \quad (26)$$

and using the electric field continuity condition at R_p and the orthogonality of the series, we have

$$b_{p,n} = 2\beta_n \frac{4\pi}{c} I_c \int_{r,z} \frac{J_c}{I_c} f_n(r) \sin(q_n z) \frac{r}{L} dr dz, \quad (27)$$

where I_c is a source current and $f_n(r)$ is given by

$$f_n(r) = \frac{g_n(r)}{\beta_n R_p A - 2S_1 B}, \quad (28)$$

with

$$S_1 = \sum_m \frac{\beta_m^2}{D_{mn}}, \quad (29)$$

$$A = K_1(\beta_n R_s) I_1(\beta_n R_p) - I_1(\beta_n R_s) K_1(\beta_n R_p), \quad (30)$$

$$B = K_1(\beta_n R_s) I_0(\beta_n R_p) + I_1(\beta_n R_s) K_0(\beta_n R_p). \quad (31)$$

Using the mode excitation method, the electromagnetic field in the plasma region is easily determined, but the field in the outer region cannot be calculated, which is essential in obtaining the discharge impedance. To obtain the electromagnetic field in the antenna region, the wave equation should be solved also in this region.

D. Image current method

In this subsection, we determine the magnetic field component at the plasma-vacuum boundary ($b_{p,n}$) [Eq. (14)], by solving the wave equation in the antenna region. We solve the wave equation by replacing the plasma current with an artificial image current sheet (giving equivalent effects to the electromagnetic field in the antenna region) at a certain radial

position in the plasma region. This image current and $b_{p,n}$ are determined without using the results of Sec. II C.

The wave equation for the electric field in the antenna region is

$$\left(\frac{\partial^2}{\partial r^2} + \frac{1}{r} \frac{\partial}{\partial r} - \frac{1}{r^2} + \frac{\partial^2}{\partial z^2} + \kappa^2 \right) E = -i\kappa \frac{4\pi}{c} J_c. \quad (32)$$

The boundary conditions are

$$E=0 \quad \text{at } r=R_s, \quad (33)$$

and E and B_z are continuous at $r=R_p$. As in the case of the plasma region, the wave equation (32) is transformed to

$$\left(\frac{\partial^2}{\partial r^2} + \frac{1}{r} \frac{\partial}{\partial r} - \frac{1}{r^2} + \frac{\partial^2}{\partial z^2} + \kappa^2 \right) E = -i\kappa \frac{4\pi}{c} [J_c + K_{s1} \delta(r-R_e) + K_{s2} \delta(r-R_s)], \quad (34)$$

where K_{s1} is an image current density flowing at R_e ($< R_p$), and the boundary condition of Eq. (33) can be satisfied by a surface current density $K_{s2} = cB_z(R_s)/2\pi$.

Equation (34) can be solved by the mode analysis method using the Fourier-Dini series. The source current density can be represented as

$$J_c = \sum_{m,n} j_{mn} J_1 \left(\lambda_{0m} \frac{r}{R_s} \right) \sin(q_n z), \quad (35)$$

where

$$j_{mn} = \frac{4}{LR_s} \frac{I_c}{J_1^2(\lambda_{0m})} \{J_{cj}^{mn}/R_s\}, \quad (36)$$

$$\{J_{cj}^{mn}/R_s\} \equiv \int_{r,z} \left(\frac{J_c}{I_c} \right) J_1 \left(\lambda_{0m} \frac{r}{R_s} \right) \sin(q_n z) \frac{r}{R_s} dr dz. \quad (37)$$

Inserting Eq. (35) into Eq. (34) and expanding K_{s1} and B_z at R_s ,

$$K_{s1} = \sum_n K_{s1,n} \sin(q_n z), \quad (38)$$

$$B_z(R_s) = \sum_n b_{s,n} \sin(q_n z), \quad (39)$$

we obtain

$$E = \sum_{m,n} e_{mn}^{(2)} J_1 \left(\lambda_{0m} \frac{r}{R_s} \right) \sin(q_n z), \quad (40)$$

where

$$e_{mn}^{(2)} = \frac{2i\kappa}{R_s J_1(\lambda_{0m}) D_{mn}^{(2)}} \left(\frac{\{J_{cj}^{mn}/R_s\}}{J_1(\lambda_{0m})} \frac{8\pi}{LC} I_c + \frac{R_e J_1(\lambda_{0m} R_e/R_s)}{R_s J_1(\lambda_{0m})} \frac{4\pi}{c} K_{s1,n} + b_{s,n} \right), \quad (41)$$

$$D_{mn}^{(2)} = (\lambda_{0m}/R_s)^2 + q_n^2 - \kappa^2. \quad (42)$$

Applying the boundary condition of Eq. (33) to Eq. (40), the coefficient $b_{s,n}$ can be determined, and the resultant coefficient of the electric field becomes

$$\begin{aligned} e_{mn}^{(2)} = & \frac{2i\kappa}{D_{mn}^{(2)}R_s J_1(\lambda_{0m})} \left(\frac{\{j_{cj}^{mn}/R_s\}}{J_1(\lambda_{0m})} \right. \\ & - \frac{2\beta_n I_0(\beta_n R_s)}{R_s (\beta_n R_s)} \sum_m \frac{\{j_{cj}^{mn}/R_s\}}{J_1(\lambda_{0m}) D_{mn}^{(2)}} \left. \right) \frac{8\pi}{Lc} I_c \\ & + \frac{2i\kappa}{D_{mn}^{(2)}R_s J_1(\lambda_{0m})} \left(\frac{J_1(\lambda_{0m} R_e/R_s)}{J_1(\lambda_{0m})} \right. \\ & - \left. \frac{I_1(\beta_n R_e)}{I_1(\beta_n R_s)} \right) \frac{R_e}{R_s} \frac{4\pi}{c} K_{s1,n}. \end{aligned} \quad (43)$$

Since the axial magnetic field should be continuous at R_p [see Eq. (8)], the coefficient of the surface current density $K_{s1,n}$ can be obtained:

$$K_{s1,n} = \frac{c}{4\pi} \frac{K_{s11}}{K_{s12}}, \quad (44)$$

where

$$\begin{aligned} K_{s11} = & b_{p,n} - \left(\sum_m \frac{\lambda_{0m} J_0(\lambda_{0m} R_p/R_s) \{j_{cj}^{mn}/R_s\}}{(\lambda_{0m}^2 + \beta_n^2 R_s^2) J_1^2(\lambda_{0m})} \right. \\ & - \left. \frac{\beta_n R_s I_0(\beta_n R_p)}{I_1(\beta_n R_s)} \sum_m \frac{\{j_{cj}^{mn}/R_s\}}{(\lambda_{0m}^2 + \beta_n^2 R_s^2) J_1(\lambda_{0m})} \right) \frac{16\pi}{Lc} I_c, \\ K_{s12} = & \left(\sum_m \frac{\lambda_{0m} J_0(\lambda_{0m} R_p/R_s) J_1(\lambda_{0m} R_e/R_s)}{(\lambda_{0m}^2 + \beta_n^2 R_s^2) J_1^2(\lambda_{0m})} \right. \\ & - \left. \frac{I_0(\beta_n R_p) I_1(\beta_n R_e)}{2I_1(\beta_n R_s) I_0(\beta_n R_s)} \right) \frac{2R_e}{R_s}. \end{aligned}$$

With Eq. (44), the electric field is represented as a function of the source current and the magnetic field at R_p . Using the remaining condition of the electric field continuity at R_p , the coefficient of the magnetic field can be expressed as

$$b_{p,n} = b_{p1}/b_{p2}, \quad (45)$$

where

$$\begin{aligned} b_{p1} = & 2\beta_n R_p (4\pi/Lc) I_c [2\beta_n R_s I_1(\beta_n R_s) I_0(\beta_n R_s) \\ & \times (S_3 - S_5) S_2 + I_1(\beta_n R_p) I_1(\beta_n R_e) S_5 \\ & + 2\beta_n R_s I_0(\beta_n R_s) \{ \beta_n R_s I_0(\beta_n R_p) - I_1(\beta_n R_p) \} S_6 S_2 \\ & - \beta_n R_s I_0(\beta_n R_p) I_1(\beta_n R_e) S_3], \end{aligned} \quad (46)$$

$$\begin{aligned} b_{p2} = & 2S_1 [2\beta_n R_s I_1(\beta_n R_s) I_0(\beta_n R_s) S_4 \\ & - \beta_n R_s I_0(\beta_n R_p) I_1(\beta_n R_e)] \\ & - \beta_n^2 R_p R_s [2\beta_n R_s I_1(\beta_n R_s) I_0(\beta_n R_s) S_2 \\ & - I_1(\beta_n R_p) I_1(\beta_n R_e)]. \end{aligned} \quad (47)$$

Here, S_1, S_2, \dots, S_6 are sums over m and functions of n given by

$$S_2 = \sum_m \frac{1}{\lambda_{0m}^2 + \beta_n^2 R_s^2} \frac{J_1(\lambda_{0m} R_p/R_s) J_1(\lambda_{0m} R_e/R_s)}{J_1^2(\lambda_{0m})}, \quad (48)$$

$$S_3 = \sum_m \frac{1}{\lambda_{0m}^2 + \beta_n^2 R_s^2} \frac{J_1(\lambda_{0m} R_p/R_s) \{j_{cj}^{mn}/R_s\}}{J_1^2(\lambda_{0m})}, \quad (49)$$

$$S_4 = \sum_m \frac{1}{\lambda_{0m}^2 + \beta_n^2 R_s^2} \frac{\lambda_{0m} J_0(\lambda_{0m} R_p/R_s) J_1(\lambda_{0m} R_e/R_s)}{J_1^2(\lambda_{0m})}, \quad (50)$$

$$S_5 = \sum_m \frac{1}{\lambda_{0m}^2 + \beta_n^2 R_s^2} \frac{\lambda_{0m} J_0(\lambda_{0m} R_p/R_s) \{j_{cj}^{mn}/R_s\}}{J_1^2(\lambda_{0m})}, \quad (51)$$

$$S_6 = \sum_m \frac{1}{\lambda_{0m}^2 + \beta_n^2 R_s^2} \frac{\{j_{cj}^{mn}/R_s\}}{J_1(\lambda_{0m})}. \quad (52)$$

It is straightforward to show that Eqs. (27) and (45) are equivalent. Actually, the electric field in the plasma region calculated using the mode excitation method and the electric field in the antenna region calculated using the image current method are linked continuously to each other at R_p .

E. Plasma and discharge impedances

According to the Poynting theorem for harmonic fields, the impedance can be defined using field quantities [19]. The Poynting theorem is written as

$$\frac{1}{2} \int_V \vec{J}^* \cdot \vec{E} d\vec{x} + 2i\omega \int_V (w_e - w_m) d\vec{x} + \oint_S \vec{S} \cdot \hat{n} da = 0, \quad (53)$$

where \vec{J} is current density, \vec{E} electric field, $w_e = |\vec{E}|^2/16\pi$ electric field energy density, $w_m = |\vec{B}|^2/16\pi$ magnetic field energy density, $\vec{S} = \vec{E} \times \vec{B}^*/8\pi$ the Poynting vector, and \hat{n} unit vector with outward normal direction to the surface. In Eq. (53), the first term represents the rate of work done by the fields in finite volume V , the second is the stored energy rate within the electromagnetic fields, and the third is the energy flow rate in outward direction through the surface S surrounding the volume.

When only the plasma region is considered, the sum of the stored and the dissipated energy rates in the plasma is the same as the energy inflow rate through the plasma-vacuum interface. From the viewpoint of an electrical circuit, this sum can be replaced with

$$\frac{1}{2} I_c^* V = \frac{1}{2} |I_c|^2 Z_{pl}, \quad (54)$$

where I_c , V , and Z_{pl} are source current, potential difference applied to the plasma, and plasma impedance, respectively. Hence, the plasma impedance is derived as

$$Z_{pl} = - \frac{2}{|I_c|^2} \int_{S_p} \vec{S} \cdot \hat{n} da, \quad (55)$$

where S_p is the plasma-vacuum interface. After some algebra, it can be shown that

$$Z_{pl} = -\frac{1}{|I_c|^2} \frac{i\omega L}{2} \sum_{m,n} \frac{|b_{p,n}|^2}{D_{mn}}, \quad (56)$$

where $b_{p,n}$ and D_{mn} are defined in Sec. II B.

The power dissipated in the antenna can be calculated in terms of the current and electric field on the antenna and can also be represented in terms of the current and antenna impedance. Hence, the antenna impedance is

$$Z_a \equiv -\frac{1}{|I_c|^2} \int_{V_a} \vec{J}_c^* \cdot \vec{E} d\vec{x}, \quad (57)$$

where V_a is the antenna volume. Since all the power dissipated and stored in the plasma and vacuum regions is transferred through the surface surrounding the antenna, the impedance calculated from Eq. (57) is the same as the total impedance of the discharge (called discharge impedance Z_{dis}). Using the orthogonality of the Fourier-Dini series, the discharge impedance reduces to

$$Z_{dis} = -\frac{2\pi R_s}{I_c} \sum_{m,n} \{J_{cj}^{mn}/R_s\} e_{mn}^{(2)}, \quad (58)$$

where $\{J_{cj}^{mn}/R_s\}$ and $e_{mn}^{(2)}$ are defined in Sec. II D.

III. NUMERICAL RESULTS AND DISCUSSION

Since the series S_1, S_2, \dots, S_6 , especially the ones involving J_1^2 in denominators, converge very slowly, some techniques are needed to accelerate the series convergence. For this purpose we use the following identities involving series sums:

$$\sum_m \frac{1}{\lambda_{0m}^2 + \beta^2 R^2} \frac{J_1(\lambda_{0m} r/R)}{J_1(\lambda_{0m})} = \frac{1}{2\beta R} \frac{I_1(\beta r)}{I_0(\beta R)} \quad (r < R), \quad (59)$$

$$\sum_m \frac{\lambda_{0m}}{\lambda_{0m}^2 + \beta^2 R^2} \frac{J_0(\lambda_{0m} r/R)}{J_1(\lambda_{0m})} = \frac{1}{2} \frac{I_0(\beta r)}{I_0(\beta R)} \quad (r < R), \quad (60)$$

$$\sum_m \frac{J_1(\lambda_{0m} r_1/R) J_0(\lambda_{0m} r_2/R)}{\lambda_{0m} J_1^2(\lambda_{0m})} = \begin{cases} R/2r_1 & (r_2 < r_1 < R) \\ 0 & (r_1 < r_2 < R), \end{cases} \quad (61)$$

$$\sum_m \frac{J_1(\lambda_{0m} r_1/R) J_1(\lambda_{0m} r_2/R)}{\lambda_{0m} J_1^2(\lambda_{0m})} = \begin{cases} r_2/4r_1 & (r_2 < r_1 < R) \\ r_1/4r_2 & (r_1 < r_2 < R). \end{cases} \quad (62)$$

As an example of using these series, let us consider the series S_2 . If the series is rewritten as

$$S_2 = \sum_m \left(\frac{1}{\lambda_{0m}^2 + \beta_n^2 R_s^2} - \frac{1}{\lambda_{0m}^2} \right) \frac{J_1(\lambda_{0m} R_p/R_s) J_1(\lambda_{0m} R_e/R_s)}{J_1^2(\lambda_{0m})} + \frac{R_e}{4R_p} \quad (63)$$

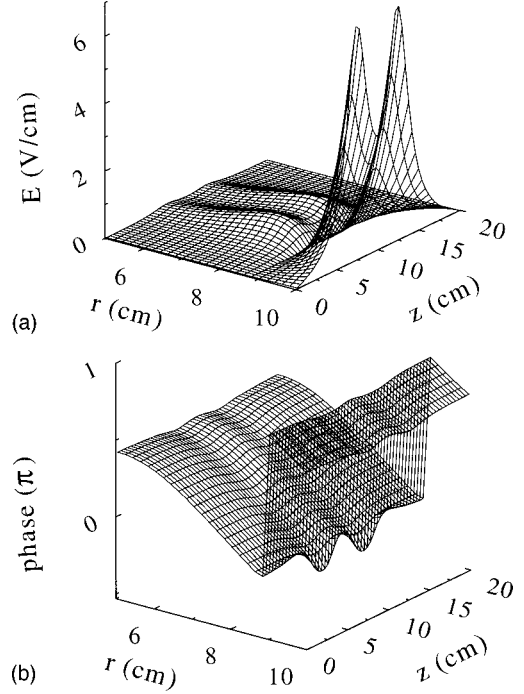


FIG. 2. Profiles of (a) amplitude and (b) phase of electric field E in the plasma.

by using Eq. (62), this new series converges faster than the original one.

In this section are presented the numerical results based on Eqs. (2)–(4), (10), (11), (56), and (58); i.e., the electric and the magnetic fields, the plasma current density, the absorption power density, and the plasma and the discharge impedances. The parameters used for the calculation are $R_s = 20$ cm, $R_p = 10$ cm, $L = 20$ cm, $n_p = 10^{12}$ cm $^{-3}$, $T_e = 5$ eV, $\omega/2\pi = 13.56$ MHz, $R_c = 11$ cm, and $z_c = 10$ cm. Here, z_c is the axial position of the antenna. The antenna coil is made of a rectangular wire loop with the cross section of 1×1 cm 2 . The collision frequency ν is set to zero. Except a parameter that is used as a variable or specially mentioned, all parameters have fixed values as set above.

In the two-dimensional space (r, z) of the plasma region with two coils located at $z = 7.5$ and 12.5 cm, the electric and the magnetic fields, plasma current density, and absorption power density are shown in Figs. 2–6. Plots of the electric field amplitude and phase are shown in Fig. 2, and there exist certain points where the electric field vanishes and the phase abruptly changes by π [18]. The magnetic field is presented in Figs. 3 and 4. The axial component of the magnetic field B_z is out of phase ($\pi/2$ faster) with the electric field (Fig. 3). The magnitude of the radial component of the magnetic field B_r is smaller than B_z . There are three nodal points in z direction, two of which are located at the coil positions and the third is at $z = L/2$ due to the boundary conditions of $E = 0$ at both $z = 0$ and $z = L$ (Fig. 4). The plasma current is nearly out of phase ($\pi/2$ later) with the electric field, since, as shown in Eq. (17), the imaginary part of the plasma conductivity is much larger than the real part in the collisionless process (Fig. 5). The absorption power density is localized at the plasma edge and there is a region where the absorption power is negative (Fig. 6).

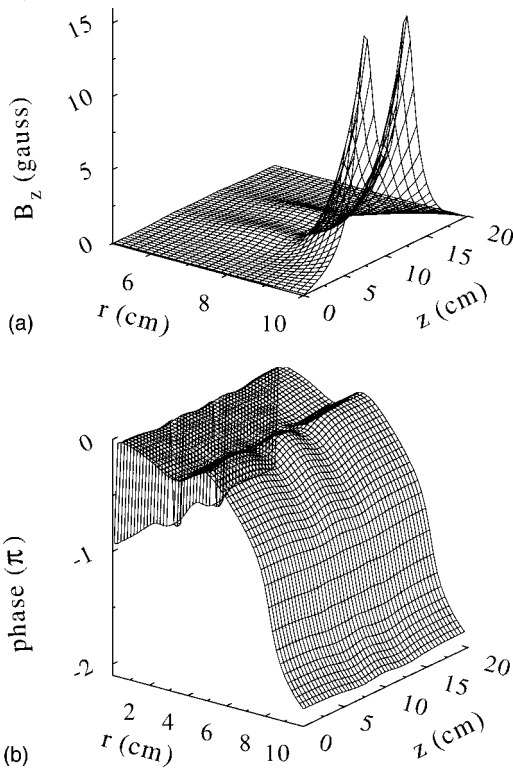


FIG. 3. Profiles of (a) amplitude and (b) phase of B_z in the plasma.

Figures 7 and 8 display the plasma resistance, which is the real part of the plasma impedance and proportional to the power deposited in the plasma. Figure 7(a) plots the plasma resistance as a function of the plasma density. The plasma resistance has a maximum value at a certain plasma density, which is similar to the results of Ref. [18], where the plasma resistance of TCP discharge is calculated. The position of the maximum point moves upward to the plasma density and its value increases as the excitation frequency becomes higher.

The dependence of the plasma resistance on the electron temperature is shown in Fig. 7(b). Since more electrons interact with the electric field as the electron temperature increases, the plasma resistance is an increasing function of the electron temperature. At a given temperature, there exists the most effective excitation frequency for heating, since the electron gains the energy through resonant coupling with the excitation wave.

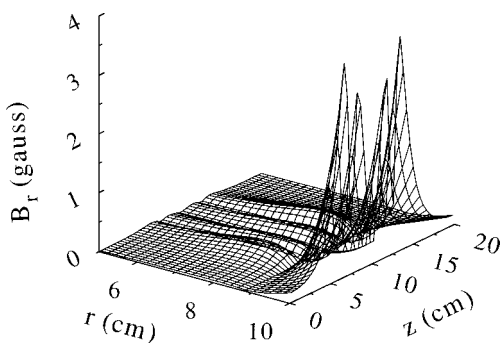


FIG. 4. Profile of amplitude B_r in the plasma.

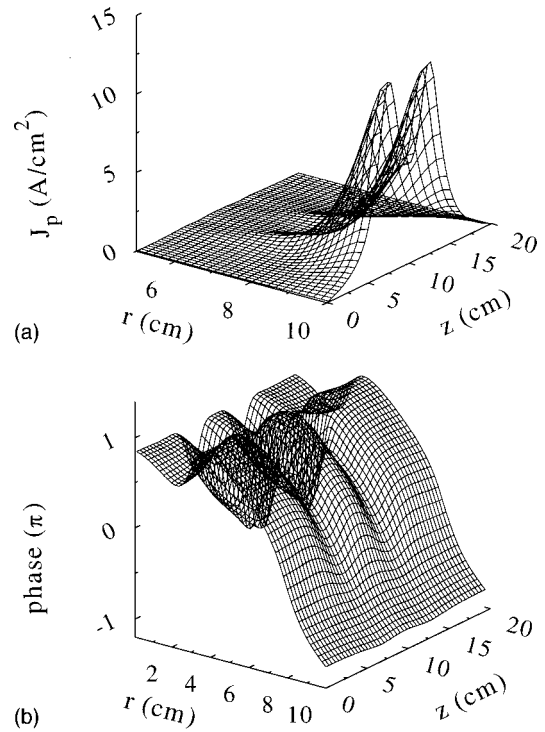


FIG. 5. Profiles of (a) amplitude and (b) phase of plasma current J_p .

In Fig. 7(c), the plasma resistance is presented as a function of the excitation frequency for various plasma densities. As is seen in Fig. 7(a) for n_p , there is a maximum plasma resistance, since the induced electric field in the plasma increases with the excitation frequency but the skin depth de-

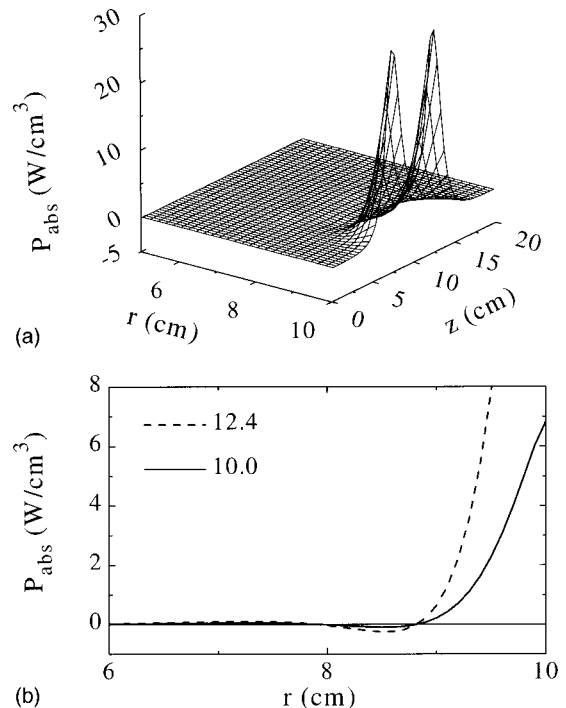


FIG. 6. Profiles of the absorption power density P_{abs} in (a) two dimensions and (b) one dimension at positions of $z=12.4$ and 10 cm.

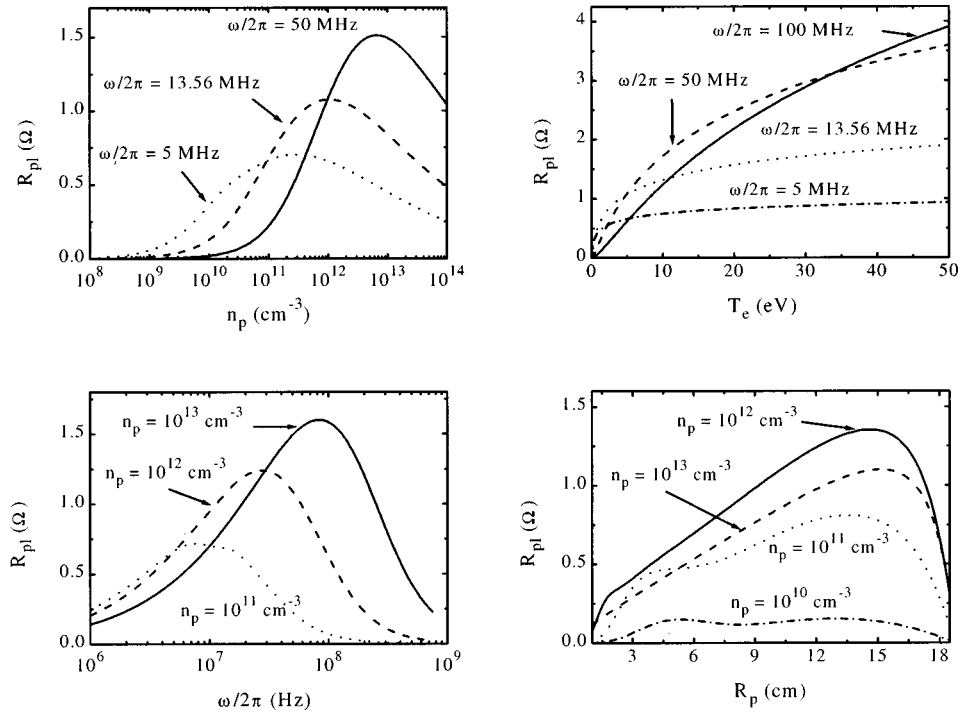


FIG. 7. Dependences of the plasma resistance R_{pl} on (a) the plasma density n_p , (b) the electron temperature T_e , (c) the excitation frequency $\omega/2\pi$, and (d) the plasma radius R_p .

creases. It is noted from Figs. 7(a) and 7(c) that there is an optimal condition of the excitation frequency for a given density.

The dependence of the plasma resistance on the plasma radius can be seen in Fig. 7(d), where the antenna radius is given as $R_p + 1$ in units of cm. There are two peaks in this plot. The first peak originates from the resonant coupling of

the electron thermal motion across the plasma diameter and the wave [17]. The second one can be explained as follows. When the plasma radius is small, the number of electrons in the skin depth increases with plasma radius. However, when the plasma radius is sufficiently large, the plasma resistance decreases rapidly, since the induced current at the chamber wall increases as the antenna moves closer to the chamber

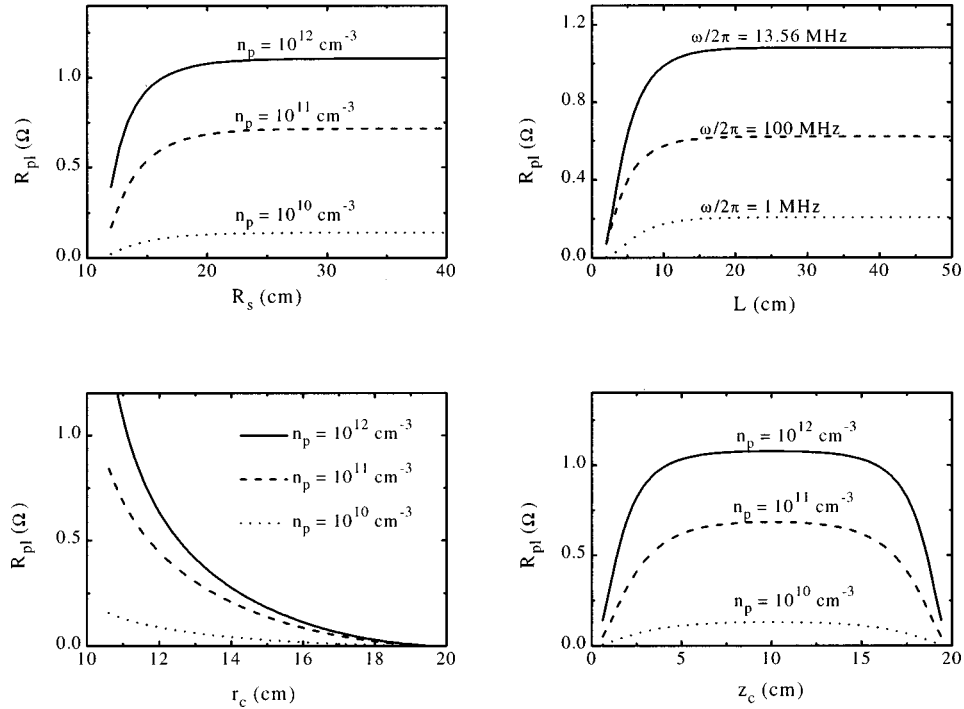


FIG. 8. Dependences of the plasma resistance R_{pl} on (a) the chamber radius R_s , (b) the plasma length L , (c) the antenna radius r_c , and (d) the axial position z_c of the antenna.

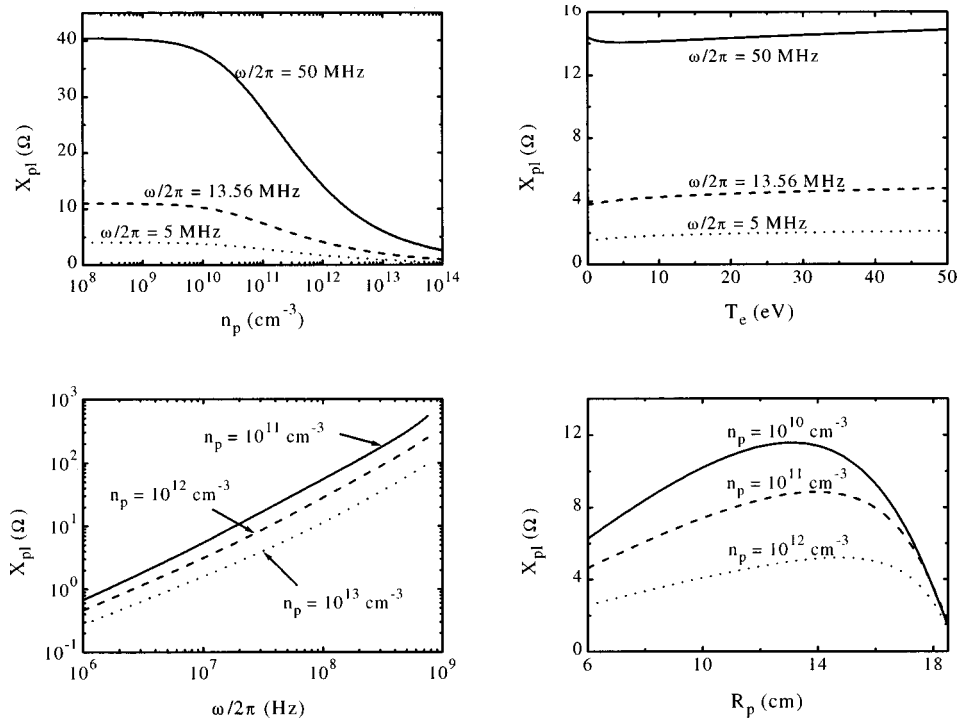


FIG. 9. Dependences of the plasma reactance X_{pl} on (a) the plasma density n_p , (b) the electron temperature T_e , (c) the excitation frequency $\omega/2\pi$, and (d) the plasma radius R_p .

wall. This induced current is out of phase with the source current, so the sum of the induced and source currents is smaller than the source current. Therefore, the induced electric field in the plasma region decreases.

The dependences of the plasma resistance on the chamber radius and on the plasma length are shown in Figs. 8(a) and 8(b), respectively. In both cases, the plasma resistance in-

creases rapidly and then becomes saturated. The reason is that the induced electric field at the chamber surface is a decreasing function of the distance between the antenna and the chamber surface. In Fig. 8(b), the antenna is positioned at the midpoint of the plasma length ($z=L/2$). As the antenna radius increases, the plasma resistance decreases, since the induced electric field at the plasma region is a decreasing

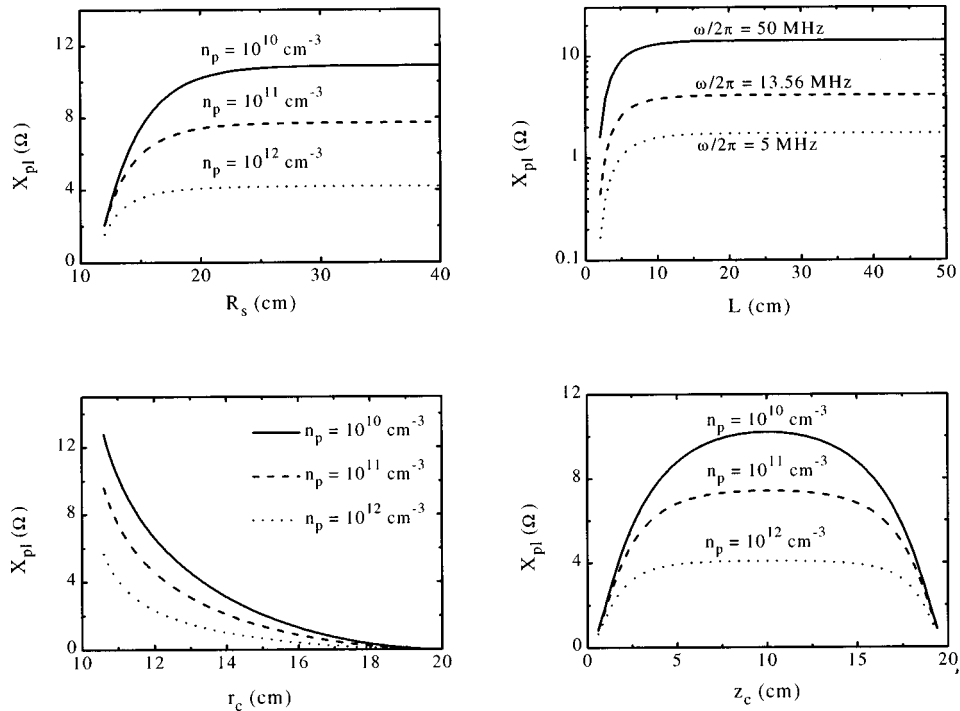


FIG. 10. Dependences of the plasma reactance X_{pl} on (a) the chamber radius R_s , (b) the plasma length L , (c) the antenna radius r_c , and (d) the axial position z_c of the antenna.

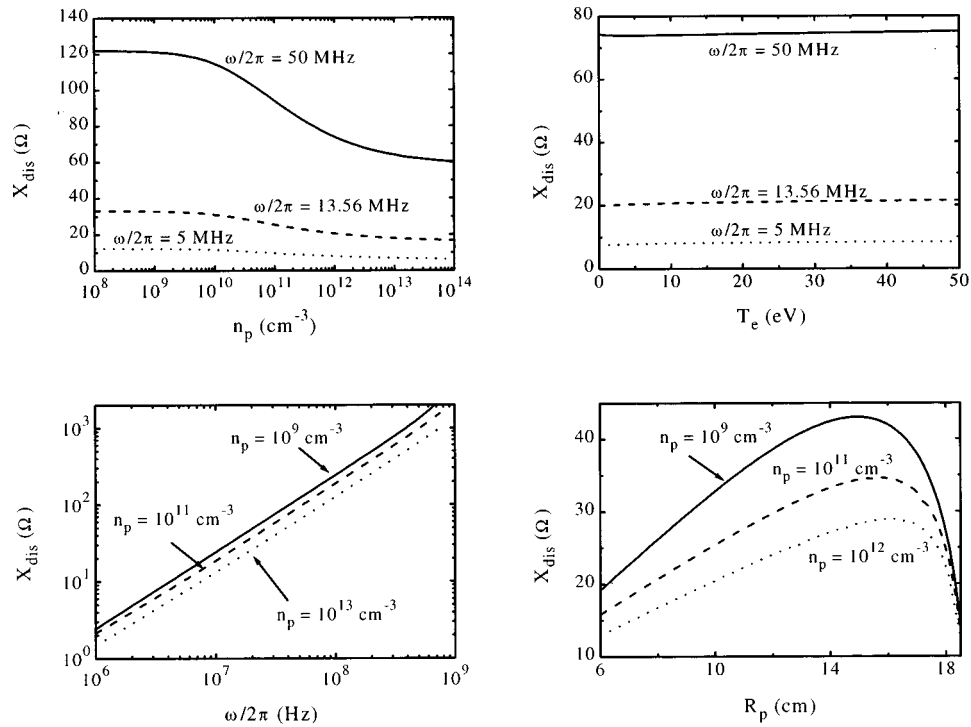


FIG. 11. Dependences of the discharge reactance X_{dis} on (a) the plasma density n_p , (b) the electron temperature T_e , (c) the excitation frequency $\omega/2\pi$, and (d) the plasma radius R_p .

function of the distance from the plasma to the antenna [Fig. 8(c)]. The plasma resistance has a maximum plateau when the antenna is located near the midrange of the plasma length [Fig. 8(d)].

Figures 9 and 10 show the plasma reactance which is the negative of the imaginary part of the impedance. The plasma

reactance is a decreasing function of the plasma density [Fig. 9(a)] and a somewhat increasing function of the electron temperature [Fig. 9(b)]. As the excitation frequency is increased, the plasma reactance increases rapidly [Fig. 9(c)]. This shows that the main component of the plasma reactance is the inductive part proportional to the wave frequency. Fig-

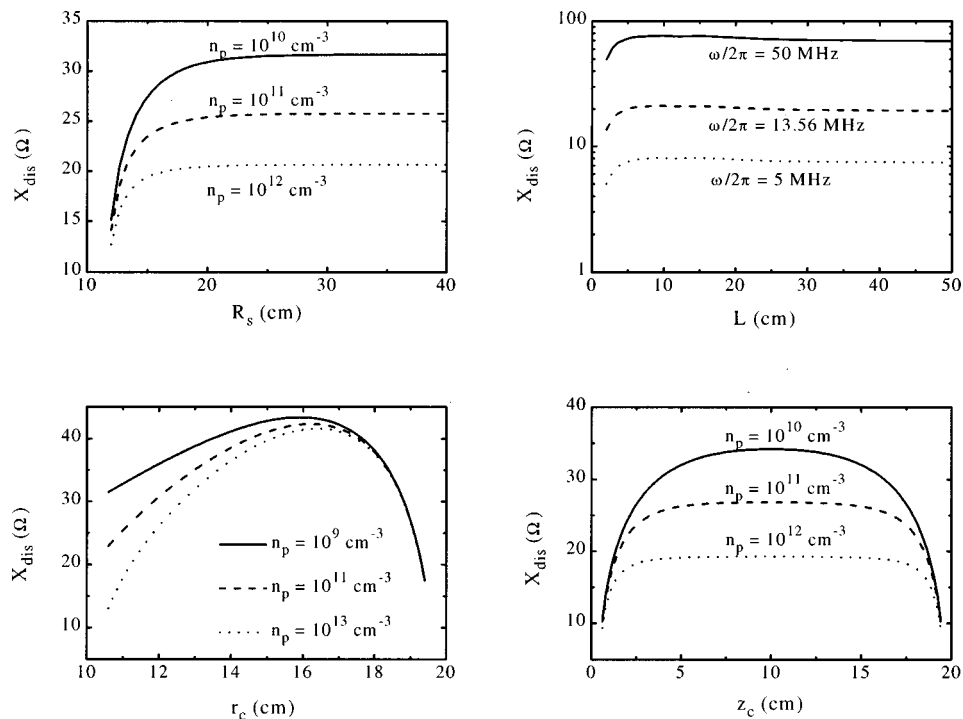


FIG. 12. Dependences of the discharge reactance X_{dis} on (a) the chamber radius R_s , (b) the plasma length L , (c) the antenna radius r_c , and (d) the axial position z_c of the antenna.

ure 9(d) indicates that the plasma reactance is an increasing function of the plasma radius. In Fig. 10, it is seen that the dependence of the plasma reactance on the chamber geometry is similar to that of the plasma resistance. Since the plasma reactance is related to the power stored in a form of electromagnetic field, the magnitude of the induced electric field in the plasma region, which depends on the geometrical factors, can explain the dependence of the plasma reactance on the geometrical factors.

The discharge reactance, which is the imaginary part of the discharge impedance and the sum of the plasma and antenna reactances, is shown as a function of the various parameters in Figs. 11 and 12. Since the antenna reactance is much larger than that of the plasma, the discharge reactance is affected mainly by the antenna reactance. The antenna coil is assumed to have no resistance, hence the discharge resistance is the same as the plasma resistance. The discharge reactance decreases with the plasma density [Fig. 11(a)] but does not vary with the electron temperature [Fig. 11(b)]. The main component of the discharge reactance is also the inductive part [Fig. 11(c)]. When the antenna is far from the chamber wall, the discharge reactance increases with the antenna radius [Figs. 11(d) and 12(c)] but is not a function of the antenna position in z direction [Fig. 12(d)]. When the antenna radius is too large, the reactance decreases [Figs. 11(d) and 12(c)] because of the induced electric field in the chamber wall. The reactance is saturated as the chamber radius and plasma length become larger [Figs. 12(a) and 12(b)].

IV. SUMMARY

The discharge and plasma impedances of a solenoidal inductively coupled plasma discharge are calculated by a mode analysis technique. To calculate the discharge impedance, the electric and magnetic fields are determined in the entire chamber. The anomalous skin effect is included in the plasma conductivity and the antenna current is realistically modeled. The discharge and plasma impedances are functions of plasma density, electron temperature, excitation frequency, chamber geometrical factors, and geometry of antenna coils.

The anomalous skin effect is related to the thermal motion of electrons, and the thermal motion is included only in the radial direction in this work. For more accurate calculation of the anomalous skin effect, the thermal motion in the axial direction should also be considered. For the self-consistent determination of plasma parameters of density and temperature, the energy and particle transport equations should be solved. These subjects are under investigation and the results will be reported elsewhere.

ACKNOWLEDGMENT

This work was supported by the Korean Ministry of Science and Technology.

-
- [1] J. W. Denneman, *J. Phys. D* **23**, 293 (1990).
 - [2] B. W. Yu and S. L. Girshick, *J. Appl. Phys.* **69**, 656 (1991).
 - [3] R. B. Piejak, V. A. Godyak, and B. M. Alexandrovich, *Plasma Sources Sci. Technol.* **1**, 179 (1992).
 - [4] G. G. Lister and M. Cox, *Plasma Sources Sci. Technol.* **1**, 67 (1992).
 - [5] V. A. Godyak, R. B. Piejak, and B. M. Alexandrovich, *Plasma Sources Sci. Technol.* **3**, 169 (1994).
 - [6] T. Sakuta, S. Oguri, T. Takashima, and M. I. Boulos, *Plasma Sources Sci. Technol.* **2**, 67 (1993).
 - [7] V. I. Kolobov, G. J. Parker, and W. N. G. Hitchon, *Phys. Rev. E* **53**, 1110 (1996).
 - [8] V. I. Kolobov and W. N. G. Hitchon, *Phys. Rev. E* **52**, 972 (1995).
 - [9] V. I. Kolobov and D. J. Economou, *Plasma Sources Sci. Technol.* **6**, R1 (1997).
 - [10] P. L. G. Ventzek, T. J. Sommerer, R. J. Hoekstra, and M. J. Kushner, *Appl. Phys. Lett.* **63**, 605 (1993).
 - [11] P. L. G. Ventzek, T. J. Sommerer, R. J. Hoekstra, and M. J. Kushner, *J. Vac. Sci. Technol. B* **12**, 461 (1994).
 - [12] R. A. Stewart, P. Vitello, and D. B. Graves, *J. Vac. Sci. Technol. B* **12**, 478 (1994).
 - [13] A. P. Paranjpe, *J. Vac. Sci. Technol. A* **12**, 1221 (1994).
 - [14] G. DiPeso, V. Vahedi, D. W. Hewett, and T. D. Rognlien, *J. Vac. Sci. Technol. A* **12**, 1387 (1994).
 - [15] M. M. Turner, *Phys. Rev. Lett.* **71**, 1844 (1993).
 - [16] M. A. Lieberman and V. A. Godyak, *IEEE Trans. Plasma Sci.* **26**, 955 (1998).
 - [17] N. S. Yoon, S. S. Kim, C. S. Chang, and D. I. Choi, *Phys. Rev. E* **54**, 757 (1996).
 - [18] N. S. Yoon, S. M. Hwang, and D. I. Choi, *Phys. Rev. E* **55**, 7536 (1997).
 - [19] J. D. Jackson, *Classical Electrodynamics* (John Wiley & Sons, New York, 1975).
 - [20] Y. S. Sayasov, *Helv. Phys. Acta* **52**, 288 (1979).
 - [21] G. N. Watson, *A Treatise on the Theory of Bessel Functions*, 2nd ed. (Cambridge, London, 1966).
 - [22] B. D. Fried and S. D. Conte, *The Plasma Dispersion Function* (Academic, New York, 1961).